Cardiovascular Engineering and Technology, Vol. 10, No. 1, March 2019 *(© 2018)* pp. 136–154
https://doi.org/10.1007/s13239-018-00396-w

Patient-Specific Multi-Scale Model Analysis of Hemodynamics Following the Hybrid Norwood Procedure for Hypoplastic Left Heart Syndrome: Effects of Reverse Blalock–Taussig Shunt Diameter

ANDRES CEBALLOS,[1] RAY PRATHER,[1] EDUARDO DIVO,[2] ALAIN J. KASSAB,[1] and WILLIAM M. DECAMPLI[3,4]

[1]Mechanical and Aerospace Engineering, University of Central Florida, Orlando, FL, USA; [2]Mechanical Engineering, Embry-Riddle Aeronautical University, Daytona Beach, FL, USA; [3]The Heart Center, Arnold Palmer Hospital for Children, Orlando, FL, USA; and [4]College of Medicine, University of Central Florida, Orlando, FL, USA

(Received 20 July 2018; accepted 20 November 2018; published online 4 December 2018)

Associate Editor Dr. Ajit P. Yoganathan and Dr. Alison Marsden oversaw the review of this article.

Abstract

Introduction—The hybrid Norwood (HN) is a relatively new first stage palliative procedure for neonates with hypoplastic left heart syndrome, in which a sustainable uni-ventricular circulation is established in a less invasive manner than with the standard Norwood procedure. A computational multi-scale model of the circulation following the HN procedure was used to obtain detailed hemodynamics. Implementation of a reverse-BT shunt (RBTS), a synthetic bypass from the main pulmonary to the innominate artery placed to counteract aortic arch stenosis, and its effects on local and global hemodynamics were studied.

Methods—A post-op patient-derived anatomy of the HN procedure was utilized with varying degrees of distal arch obstruction, or stenosis, (nominal and 90% lumenal area reduction) and varying RBTS diameters (3.0, 3.5, 4.0 mm). A closed lumped parameter model (LPM) for the proximal and peripheral circulations was coupled to a 3D computational fluid dynamics (CFD) model in order to obtain converged flow fields for analysis.

Results—CFD analyses of patient-derived anatomic configurations demonstrated consistent trends of vascular bed perfusion, vorticity, oscillatory shear index and wall shear stress levels. In the models with severe stenosis, implementation of the RBTS resulted in a restoration of arterial perfusion to near-nominal levels regardless of the shunt diameter. Shunt flow velocity, vorticity, and overall wall shear stress levels decreased with increasing shunt diameter, while shunt flow and systemic oxygen delivery increased with increased shunt diameter. In the absence of distal arch stenosis, large (4.0 mm) grafts may risk thrombosis due to low velocities and flow patterns.

Conclusion—Among the three graft sizes, the best option seems to be the 3.5 mm RBTS which provides a more organized flow similar to that of the 3.0 mm configuration with lower levels of wall shear stress. As such, in the setting of this study and for comparable HN physiologies our results suggest that: (1) the 4.0 mm shunt is a generous shunt diameter choice that may be problematic particularly when implemented prophylactically in the absence of stenosis, and (2) the 3.5 mm shunt may be a more suitable alternative since it exhibits more favorable hemodynamics at lower levels of wall shear stress.

Keywords—HLHS, Hybrid Norwood, Reverse Blalock–Taussig shunt, Stenosis, CFD, LPM.

INTRODUCTION

Hypoplastic left heart syndrome (HLHS) is a complex type of congenital heart disease that occurs in 1 per 5000 births.[18] It presents itself as underdeveloped structures in the left side of the heart. Without surgical intervention, HLHS is fatal within the first hours or days after birth as the severely malformed anatomies of the left ventricle, mitral and aortic valves, and ascending aorta cannot meet the body's needs. The hybrid Norwood (HN) procedure, involves a less invasive strategy than conventional treatment to establish a uni-ventricular circulation. The HN procedure avoids cardiopulmonary bypass (heart–lung machine), deliberate cardiac arrest, and circulatory arrest of the patient during the procedure. The procedure consists of branch pulmonary artery banding, stenting of the ductus arteriosus, and balloon atrial septostomy if required. The less invasive nature of the HN and deferment of the risk of major open heart surgery to an older age are considered to help improve survival as well as neurological and cardiac functional outcomes.[1,7,15,30] The resulting systemic-pulmonary cir-

Address correspondence to Ray Prather, Mechanical and Aerospace Engineering, University of Central Florida, Orlando, FL, USA. Electronic mail: wram2@knights.ucf.edu

culation is unconventional; blood is pumped simultaneously and in parallel to the systemic and pulmonary arteries after the procedure. This circulation is complex and is yet to be fully understood. The HN procedure has its unique set of complications that may arise during postoperative care, of which one of the most important is obstruction in the aortic isthmus. This can occur immediately as a result of stent maldeployment or later due to neointimal remodeling or fibrosis. Clinically important obstruction of the distal aortic arch has been reported to occur in 24% of patients after hybrid procedures for HLHS.[30] It has been suggested that, in patients that develop distal aortic arch obstruction, placement of a reverse Blalock–Taussig shunt (RBTS, main pulmonary artery-to-innominate artery shunt) could prevent myocardial and cerebral ischemia.[8] The RBTS is a straightforward surgical addition to the HN and, although benefits of implementing this step remain unproven, some have adopted the policy of placing this shunt as a prophylactic measure in patients with limited or absent antegrade aortic flow, or at high risk of developing aortic arch obstruction.[8] Computational fluid dynamics (CFD) is being successfully used to elucidate the optimal approach to staged reconstruction of HLHS.[3,6,10,13,19,21,22,25–27] In our earlier work,[10] we utilized a synthetic geometry representative of an HLHS patient treated with HN palliation to investigate the efficacy of the RBTS to restore flow and provide adequate coronary perfusion under the conditions of moderate to severe arch stenosis and we considered a single 4 mm shunt diameter. The current study employs a patient-derived geometry and explores and compares the hemodynamics resulting from three shunt diameters in the context of prophylactic use of the RBTS or in the presence of severe distal arch stenosis. In addition, the present manuscript includes quantifications of systemic oxygen deliveries. Specifically, we extend our investigation by using a multi-scale CFD model coupling a detailed three-dimensional (3D) model of the pulsatile hemodynamics of the HN driven by a lumped parameter (0D) model of the peripheral circulation to explore the flow characteristics of various diameter RBTS of 3, 3.5, and 4 mm RBTS in the presence or absence of distal arch stenosis and the corresponding cerebral and coronary perfusion under such range of conditions.

MATERIALS AND METHODS

In order to study the complex circulation and the effects of shunt size and placement, a multi-scale CFD model of the neonatal HN circulation was developed utilizing a 0D electrical lumped parameter model (LPM) for the peripheral circulation coupled with a 3D CFD model that allows detailed computation of the local pulsatile hemodynamics.

Anatomical Model

A post HN procedure patient-derived anatomy was reconstructed from magnetic resonance imaging (MRI) data using medical image segmentation software (Mimics, Materialise, Belgium) to include atresia of the aortic valve and including the ascending aorta, transverse arch (TA), innominate artery (IA), right and left subclavian arteries (RSA, LSA), right and left carotid arteries (RCA, LCA), main pulmonary artery (MPA), branched pulmonary arteries (BPA, right = RPA, left = LPA), patent ductus arteriosus (PDA), descending aorta (DA), and right and left coronary arteries (RcorA, LcorA). The present study, provides insight into the HN flow patterns and focuses on shunt flow under multiple RBTS diameters motivated by a recent study by Baba *et al.*[2] that suggests a significant trend toward more neurologic complications in stage 1 patients with RBTS compared to those after the standard HN procedure.

Eight rigid-walled models were developed for each of the patient-derived (P1–P8) anatomy, see Table 1. We considered two cases of severity of aortic arch hypoplasia. The first case, models P1, is a nominal model analogous to the standard HN procedure with "typical" hypoplasia of the proximal arch. The second case, models P2, is a stenosed model where part of the computational domain was removed at a point proximal to the PDA and distal to the LSA to decrease the lumen of the transverse aortic arch (90%) representing a severe stenosis. Models P3–P8 were constructed by incorporating a 3.0, 3.5 or 4.0 mm in diameter by 21 mm in length bypass graft (RBTS) from the MPA to the IA as shown in Figs. 1, 2 and Table 1. The RBTS dimensions are representative of a graft typically used for this procedure. In the patient-derived models, the coronary arteries were

TABLE 1. Eight models of each of the patient-derived derived anatomical configuration (P1–8).

Baseline model	RBTS diameter × length added to baseline models		
Patient-derived nominal (P1)	3 mm × 21 mm RBTS (P3)	3.5 mm × 21 mm RBTS (P4)	4 mm × 21 mm RBTS (P5)
Patient-derived 90% stenosed (P2)	3 mm × 21 mm RBTS (P6)	3.5 mm × 21 mm RBTS (P7)	4 mm × 21 mm RBTS (P8)

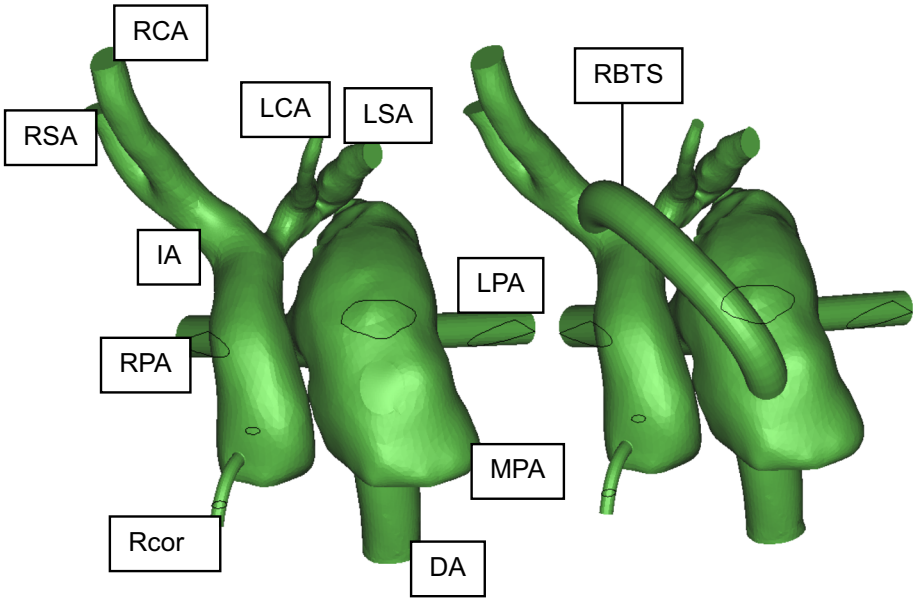

FIGURE 1. Patient derived anatomical configurations: 90% stenosis shown without RBTS (left) and with RBTS (right). Frontal view. Labels indicate vessel of concern and shunt locations.

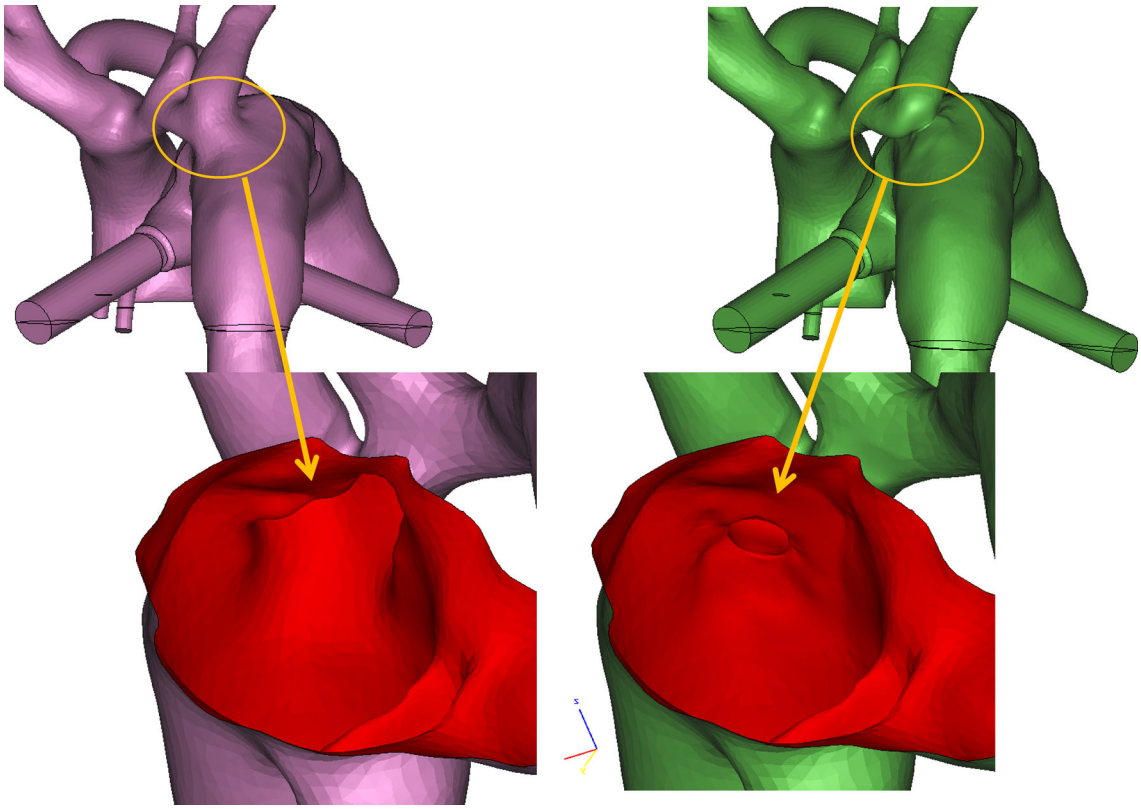

FIGURE 2. Patient derived anatomy nominal anatomy (left) and with 90% stenosis (right). Posterior view.

modeled synthetically from their take off of the ascending aorta because the resolution and contrast of the MRI did not allow for an accurate reconstruction. The length of the pulmonary arteries was extended and banded sections of the vessels were added synthetically due to the aforementioned reasons. The dimensions of the model are depicted in Fig. 3.

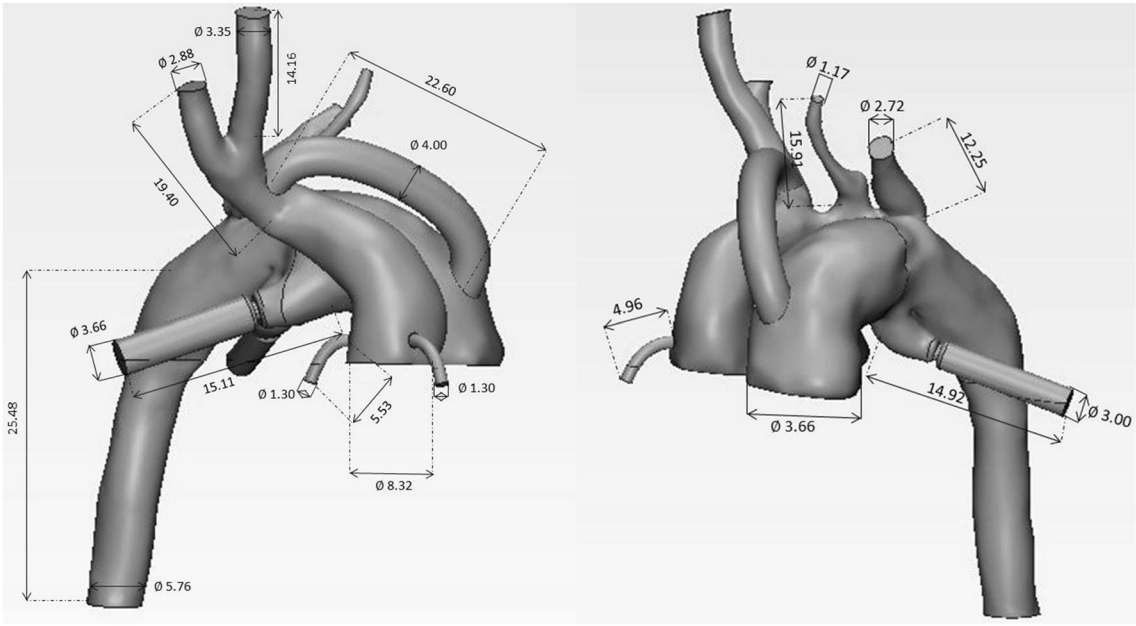

FIGURE 3. Anatomy dimensions in millimeters (Ø = diameter). Patient derived model in Nominal 4.0 mm RBTS configuration, lateral (left) and coronal (right) views.

CFD Model

The fluid domain models were imported into Star-CCM + (CD-Adapco, NY), a commercial Finite Volume-based CFD software. A high- quality mesh was obtained for all models providing grid-independence and adequate capture of the boundary layer and detailed flow features. The number of finite volumes used varied in the range between 1 and 3.1 million, depending on the anatomy. Blood was modeled as an incompressible Newtonian fluid with density of $\rho = 1060$ kg/m^3 and viscosity of $\mu = 0.004$ Pa-s. The 3D flow field is obtained by numerically resolving the Navier–Stokes mass and momentum conservation equations:

$$\nabla \cdot \vec{V} = 0 \tag{1}$$

$$\rho \frac{\partial \vec{V}}{\partial t} + \rho(\vec{V} \cdot \nabla)\vec{V} = -\nabla p + \mu \nabla^2 \vec{V} \tag{2}$$

Here, $\vec{V}$ is the velocity vector and p is the pressure field. The Navier–Stokes equations were solved with an unsteady implicit scheme. The time step of 4.62 ms provided time-independent solution for a 130 bpm. Waveforms provided by a 0D LPM of the circulation are used to impose an unsteady stagnation pressure inlet at the MPA root and prescribe unsteady mass flow rates as arterial outlet boundary conditions (BCs).

Lumped Parameter Model

The LPM is an electrical analog of the circulatory system[31] modeling viscous drag as a resistor (R), flow inertia as an inductor (L), vessel compliance as a capacitor (C), and tricuspid and pulmonary valves as ideal diodes to impose unidirectional flow. A pair of differential equations governs each R–L–C compartment model of a vascular bed:

$$\Delta p = L\frac{dQ}{dt} + RQ$$

$$Q = C\frac{dp}{dt}, \tag{3}$$

where Q is the flow-rate and Δp is the pressure difference, while the second equation models vessel wall compliance with. Baseline values of R, L, and C were obtained from the literature.[6,21,25,26] These were adjusted iteratively to approach waveforms from catheterization data of a "typical" HN patient. Clinically, obtaining pressure or flow waveforms for all the required vessels in neonates is not feasible using the standard catheterization methods, thus tuning of the model relies to a degree in medical judgement of the appropriate net flow rates and target pressures. The main parameters that are initially tuned in the present study, for which clinical data is available are: cardiac output, ventricular pressure, atrial pressure, DA pres-

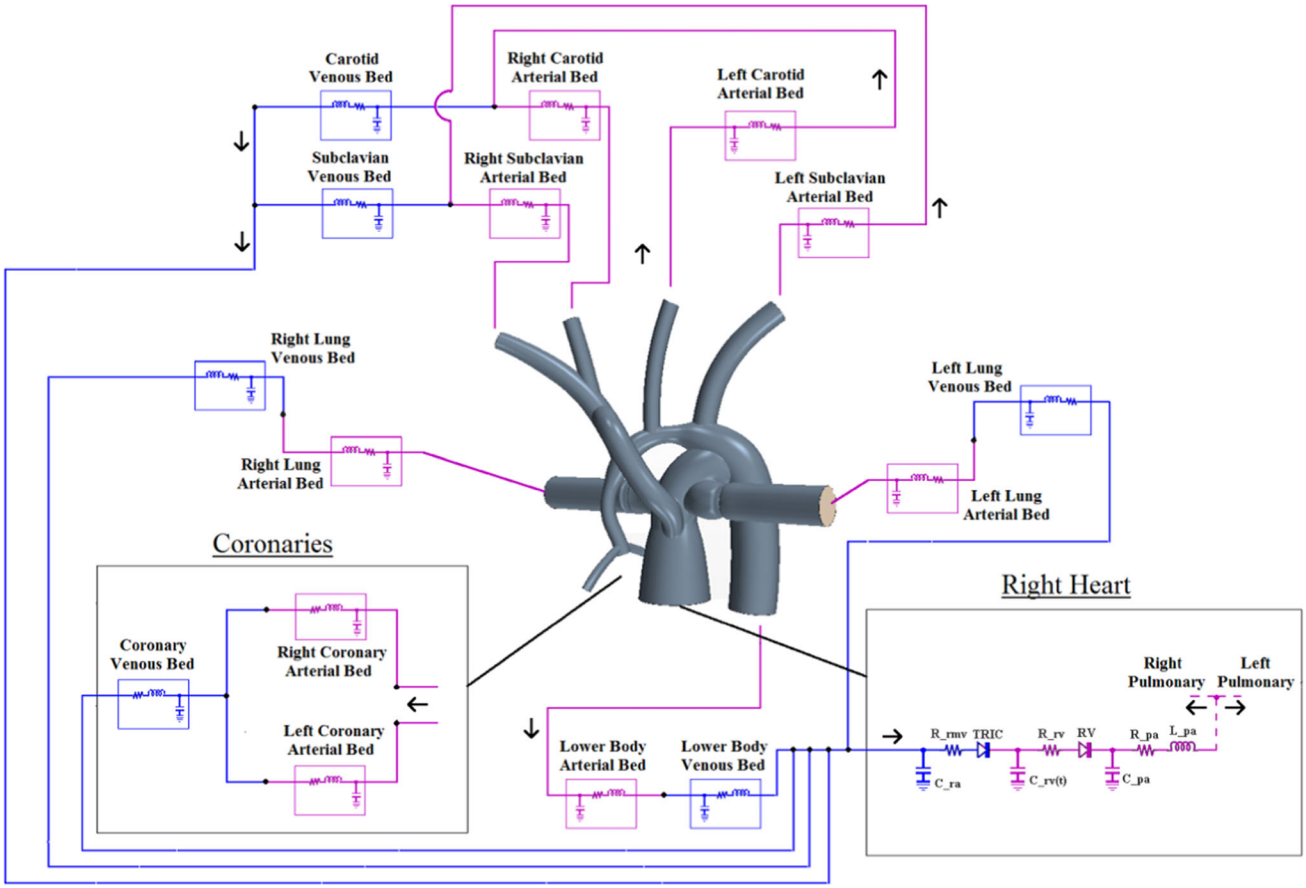

FIGURE 4. Multi-scale model of the HN circulation, three-dimensional CFD model coupled with lumped parameter model. A synthetic HN anatomy shown for illustrative purposes.

sure, and branched pulmonary arterial pressure. The arterial vascular bed resistance is tuned first, since it is the primary determinant of total flow through any given artery. Compliance and inductance parameters are then tuned to approach the desired waveform.

The right ventricle, modeled as a time-varying capacitor $C(t)$, is the driving force of the circuit providing pulsatile cardiac output. Its reciprocal, the elastance function $E_n(t_n)E(t)$, relates ventricular pressure and volume at a given point during the cardiac cycle. The form $E(t) = (E_{\max} - E_{min}) \cdot E_n(t_n) + E_{\min}$ was used, where, $E_n(t_n)$ is the "double hill" normalized elastance function which has been modified from the adult model in Simaan *et al.*[29] to a neonate model as:

$$E_n(t_n) = \left[\frac{\left(\frac{t_n}{0.303}\right)^{1.32}}{1 + \left(\frac{t_n}{0.303}\right)^{1.32}}\right]\left[\frac{1}{1 + \left(\frac{t_n}{0.508}\right)^{21.9}}\right], \quad (4)$$

where $E_{\max} = 2.35$ and $E_{\min} = 0.06$ regulate the bounds of the function based on the period-normalized time quantity $t_n = \frac{t}{t_c}$ with $t_c = \frac{60}{HR}$ (HR is the heart rate). The exponential coefficients in Eq. (4) were adjusted iteratively to produce a cardiac output for the nominal model of approximately 2.0 L/min. These values were held constant for all subsequent simulations. The right atrium was modeled using a constant elastance. A 32 degree of freedom (DOF) closed-loop circuit representation of the systemic and pulmonary circulation (Fig. 4) leads to system of coupled ordinary differential equations that are solved *via* a 4th order adaptive Runge–Kutta integrator.

BPA banding is achieved using a geometrical restriction in the CFD model supplemented with a resistance placed in pulmonary LPM vascular bed to achieve cycle-averaged ratio of total BPA artery to ductal flow, $Q_p/Q_s \sim 1$, in the nominal model. Earlier computational models[26] show that a Q_p/Q_s ratio of one is optimal in first stage single ventricle palliative procedures, thus, the current model is adjusted to represent a pulmonary banding procedure that achieves this parameter closely. The effect of different levels of pulmonary banding restriction will likely only influence localized flow in the banding region (since $Q_p/Q_s \sim 1$) and therefore this variable was not considered in the study. In order for the LPM to account for most of the coronary perfusion during diastole, the

coronary arterial bed resistance was assumed to be a normalized polynomial function of the time-varying elastance (see Eq. (5) below). The nominal LPM parameters are held constant in subsequent simulations in which the RBTS, as well as a 90% discrete stenosis of the isthmus, are incorporated to the 3D model.

$$R_{coronary} = K\left(\frac{E(t)}{E_{min}}\right)^2 \tag{5}$$

where $E(t)$ is as determined from Eq. (4). The constant, $K = 1.75$, was modified arbitrarily to achieve the proper coronary flow rate in the nominal case, then left unmodified for subsequent iterations.

Coupling

Coupling refers to the interaction between the Lumped Parameter and the CFD models. A baseline LPM of the Nominal anatomical configuration is constructed and adjusted to approach pressure waveforms derived from a catheterization procedure performed on a typical HN patient. This baseline LPM model is tuned as described below, with all vascular bed parameters influencing the output waveforms. The cycle total flow values of the LPM are matched within 1% for patient derived anatomies in the nominal case. In all other anatomical configurations the coupling only affects those parameters that are common in the LPM and CFD, that is, the parameters in the arterial and venous beds remain constant. This is done to obtain a relative comparison of results among the anatomical configurations; no considerations were given to physiological responses affecting vascular resistance. The coupling is achieved by: (1) tuning the initial LPM circuit to produce flow and pressure waveforms that match those obtained from catheterization or supplemental data of nominal values for typical HLHS patients, (2) imposing transient BCs to the CFD model from the circuit, (3) carrying out the CFD simulation to obtain the detailed flow field, (4) modifying the CFD equivalent parameters within the circuit to match those derived from the CFD, (5) running the LPM and imposing updated BCs to CFD, and (6) iterating the system of equations until convergence. Convergence is achieved once the relative change in flow rates at all branch vessels across each iteration is less than 10^{-2}. It is reached typically within 15–20 coupling-iterations. Once the process has converged, the CFD simulation is run for three cardiac cycles to achieve a sustained periodic solution, and post-processing is performed. Our iterative approach provides a convenient and computationally effective way to tune the LPM parameters.

Oxygen Transport Model

The oxygen transport model is based on the typical uptake, consumption, and conservation equations used in physiology, implemented in the present study using the LPM model. Oxygen transport equations are not calculated for the CFD model since the oxygen concentration entering the pulmonary and systemic arteries is the same in the HN anatomy. The major driver for systemic and pulmonary oxygen concentrations is thus the pulmonary to systemic blood flow ratio (Q_p/Q_s). The premise of the LPM oxygen transport model can be described using the following equations,

$$C_{P,venO_2} \cdot Q_p = C_{P,artO_2} \cdot Q_P + S\dot{V}_{O_2} \tag{6}$$

$$C_{S,venO_2} \cdot Q_S = C_{S,artO_2} \cdot Q_S - C\dot{V}_{O_2} \tag{7}$$

Equation (6) states that the oxygen flow into the pulmonary veins, $C_{P,venO_2} \cdot Q_p$, is equal to the oxygen flow entering the pulmonary arterial circulation, $C_{P,artO_2} \cdot Q_P$, plus the oxygen uptake in the lungs, $S\dot{V}_{O_2}$. Equation (7) states that the oxygen flow out of the systemic venous circulation, $C_{S,venO_2} \cdot Q_S$, is equal to flow of oxygen entering the systemic arterial circulation $C_{S,artO_2} \cdot Q_S$, minus the whole-body oxygen consumption, $C\dot{V}_{O_2}$. The analysis will assume steady state conditions (maintaining constant oxygen concentration in time), therefore according to the mass conservation for oxygen,

$$S\dot{V}_{O_2} = C\dot{V}_{O_2} \tag{8}$$

The systemic oxygen delivery is thus a function of cardiac output (CO), Q_p/Q_s, pulmonary venous blood oxygen delivery, and the whole-body oxygen consumption as follows,

$$C_{S,artO_2} \cdot Q_s = C_{P,venO} \cdot \frac{CO}{\frac{Q_p}{Q_s} + 1} - C\dot{V}_{O_2} \cdot \frac{1}{\frac{Q_p}{Q_s}} \tag{9}$$

$$C_{P,venO_2} = P \cdot Sat * \gamma \tag{10}$$

where γ is the blood oxygen capacity defined as 0.22 (mL oxygen/mL blood), $P \cdot Sat$ is the pulmonary venous flow oxygen saturation defined as 96%, and the whole-body oxygen consumption, $C\dot{V}_{O_2}$, as 18 (mL oxygen/min) for a neonate.[4]

Hemodynamic Parameters

Hemodynamics are investigated in post-processing by examining the velocity vectors, by computing the wall shear stress (WSS), and by computing the oscillatory shear index (OSI), an indicator of cyclic depar-

ture of the wall shear stress vector from its predominant axial alignment. The WSS and OSI are defined as:

$$\mathrm{WSS} = \left| \frac{1}{T} \int_0^T \vec{\tau}_w dt \right| \tag{11}$$

$$\mathrm{OSI} = \frac{1}{2}\left(1 - \frac{\left|\int_0^T \vec{\tau}_w dt\right|}{\int_0^T |\vec{\tau}_w| dt}\right) \tag{12}$$

where $\vec{\tau}_w$ is the instantaneous wall shear stress vector. Equation (11) is the time average of the wall shear stress magnitude.[12] In Eq. (12), the numerator of the shear stress fraction represents the magnitude of the time averaged wall shear stress while the denominator represents the time-average of the wall shear stress magnitude. The OSI can vary from 0 or no variation in the stress alignment to 0.5, a complete reversal. In addition, we studied the shunt flow vorticity ($\nabla \times \vec{V}$) which is a measure of fluid rotation in the RBTS.

RESULTS AND DISCUSSION

Pressure and flow-rate waveforms were obtained for the major arteries in all configurations. A comparison of the major phenomena in anatomical configurations with and without the RBTS was performed in our previous study for the synthetic anatomy using a 4 mm RBTS.[10] The strong effect due to the presence of stenosis and the relief introduced by the shunt can be highlighted (Table 2). In general, with 90% stenosis, the model displays a marked reduction in flow up to a 15% in branching arteries, loss in pressure and pulsatility when no shut is present. In the stenosed RBTS cases, the RBTS compensated for the distal arch obstruction, restoring cardiac output as well as coronary and arch branch flows and pressures to near nominal levels. When no stenosis is present, the shunt has little influence on flow rates of branching vessels. The effect of shunt size, though smaller in comparison, shows flow variations through the RBTS as a percentage of cardiac output up to 3% in both stenosed and non-stenosed configurations. Models including arch stenosis have lower cardiac output (up to 3.95% drop) due to the increased afterload resulting from the reduction of the isthmus lumen. Individual cycle-averaged flow rates are provided in Table 2 as a percentage of cardiac output as well as percent change from Nominal values. Cycle-averaged velocities through the shunt, as well as averaged retrograde and antegrade flow, are provided in Fig. 5.

Incorporating the RBTS in the absence of stenosis results in a slight increase in cardiac output (Table 2) of up to 1.60%. This is observed for increasingly larger shunt diameters in the nominal cases without causing significant changes in the overall flowrates and pressures. This supports the notion of implanting the shunt as a preventative measure foreseeing the possibility that stenosis may develop over time after the initial

TABLE 2. Cardiac output, arterial flow rates and relative flow changes in the patient derived anatomical configurations.

		Flow rates as percentage of cardiac output										
Patient derived	Cardiac output (mL/min)	Q_p/Q_s	DA	LCA	LcorA	LPA	LSA	RCA	RcorA	RPA	RSA	Shunt
Nominal	2022	0.95	29.2	4.7	1.8	24.3	4.7	4.7	1.7	24.4	4.6	
Nominal-3 mm RBTS	2029	0.94	29.2	4.6	1.7	24.5	4.7	4.7	1.8	24.0	4.7	10.8
Nominal-3.5 mm RBTS	2047	0.96	29.1	4.6	1.7	24.5	4.6	4.6	1.7	24.6	4.6	11.7
Nominal-4 mm RBTS	2055	0.94	29.1	4.7	1.7	24.2	4.7	4.8	1.7	24.2	4.7	13.7
Stenosed	1942	1.01	29.8	4.1	1.6	25.0	4.2	4.2	1.7	25.2	4.1	
Stenosed-3 mm RBTS	2031	0.96	29.1	4.6	1.7	24.5	4.6	4.6	1.7	24.6	4.6	15.1
Stenosed-3.5 mm RBTS	2041	0.96	29.0	4.6	1.7	24.5	4.6	4.6	1.7	24.6	4.6	16.7
Stenosed-4 mm RBTS	2051	0.96	29.0	4.6	1.7	24.5	4.6	4.6	1.7	24.6	4.6	18.1

		Percentage change from nominal									
	Cardiac output (mL/min)	Q_p/Q_s	DA	LCA	LcorA	LPA	LSA	RCA	RcorA	RPA	RSA
Nominal-3 mm RBTS	0.33	− 0.7	0.6	− 0.6	− 1.3	1.3	0.6	0.6	5.2	− 1.3	1.4
Nominal-3.5 mm RBTS	1.20	1.3	1.1	− 0.9	− 1.1	2.0	− 0.5	0.0	0.9	1.8	1.1
Nominal-4 mm RBTS	1.60	− 1.0	1.5	2.5	1.4	1.4	2.2	3.6	1.7	0.8	4.2
Stenosed	− 3.95	6.4	− 1.9	− 15.5	− 10.1	− 1.0	− 13.5	− 14.2	− 8.5	− 0.9	− 14.0
Stenosed-3 mm RBTS	0.41	1.5	0.3	− 1.8	− 1.3	1.3	− 1.6	− 1.3	− 0.4	1.1	0.1
Stenosed-3.5 mm RBTS	0.90	1.5	0.5	− 1.1	− 1.1	1.8	− 0.7	− 0.2	0.7	1.6	1.1
Stenosed-4 mm RBTS	1.40	1.3	0.9	− 0.2	0.6	2.2	0.0	0.7	− 0.1	2.0	1.6

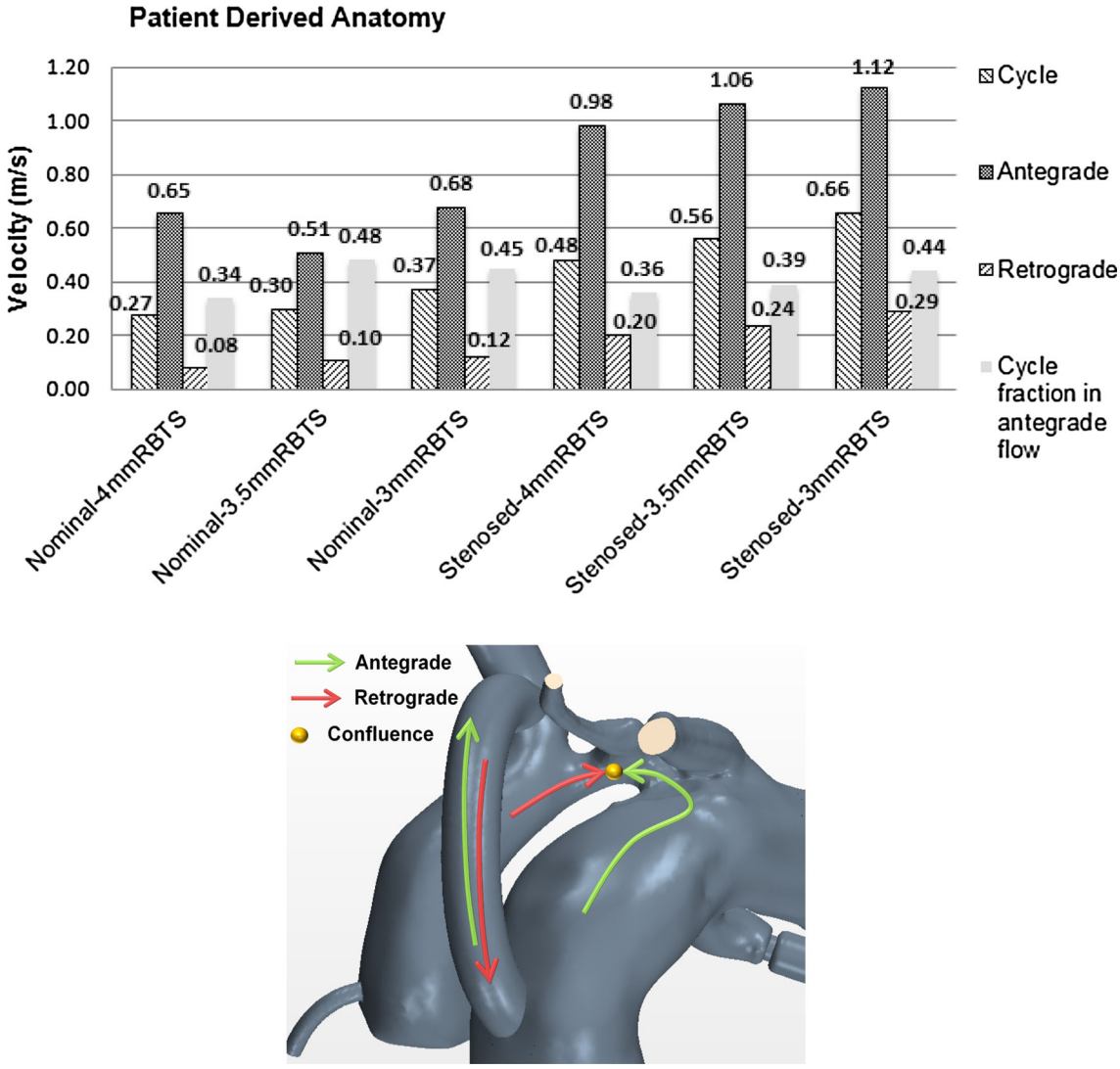

FIGURE 5. Averaged flow velocity magnitude through shunt during the cardiac cycle. Antegrade and retrograde averaged velocity magnitudes also included for the patient derived anatomical configurations with illustration of the corresponding reference nomenclature.

procedure, reducing or eliminating the need for re-intervention. However, the prophylactic use of the 4.0 mm RBTS in the absence of distal arch stenosis may have negative implications due to abnormal hemodynamic patterns that are potentially thrombogenic sites, as will be discussed below.

Patient Derived Anatomy Hemodynamics

In previous work with a synthetic Nominal 4.0 mm RBTS configuration, prominent recirculation and stagnation zones were observed, particularly at the origin of IA caused by the confluence of retrograde flow from the PDA and the RBTS through the IA, as well as at the distal anastomosis of the RBTS (Fig. 6a).[9–11] The patient-derived 90% stenosis 4.0 mm RBTS configuration exhibits more organized flow through the shunt and reduced recirculation zones (Fig. 6b). The chaotic swirling seen through the shunt in the Nominal 4.0 mm RBTS configuration is not present in the 90% stenosis configurations.[10] This is, again, a consequence of the higher flow velocity through the RBTS. Hence, careful consideration of shunt size in the absence of distal aortic arch obstruction is important, as it may result in undesirable flow conditions such as persistent stagnation and recirculation zones. Characteristically, such zones have low shear stress promoting platelet activation, aggregation and thrombosis, especially within the lumen of a synthetic graft.[5,24] The hypoplastic features of the pa-

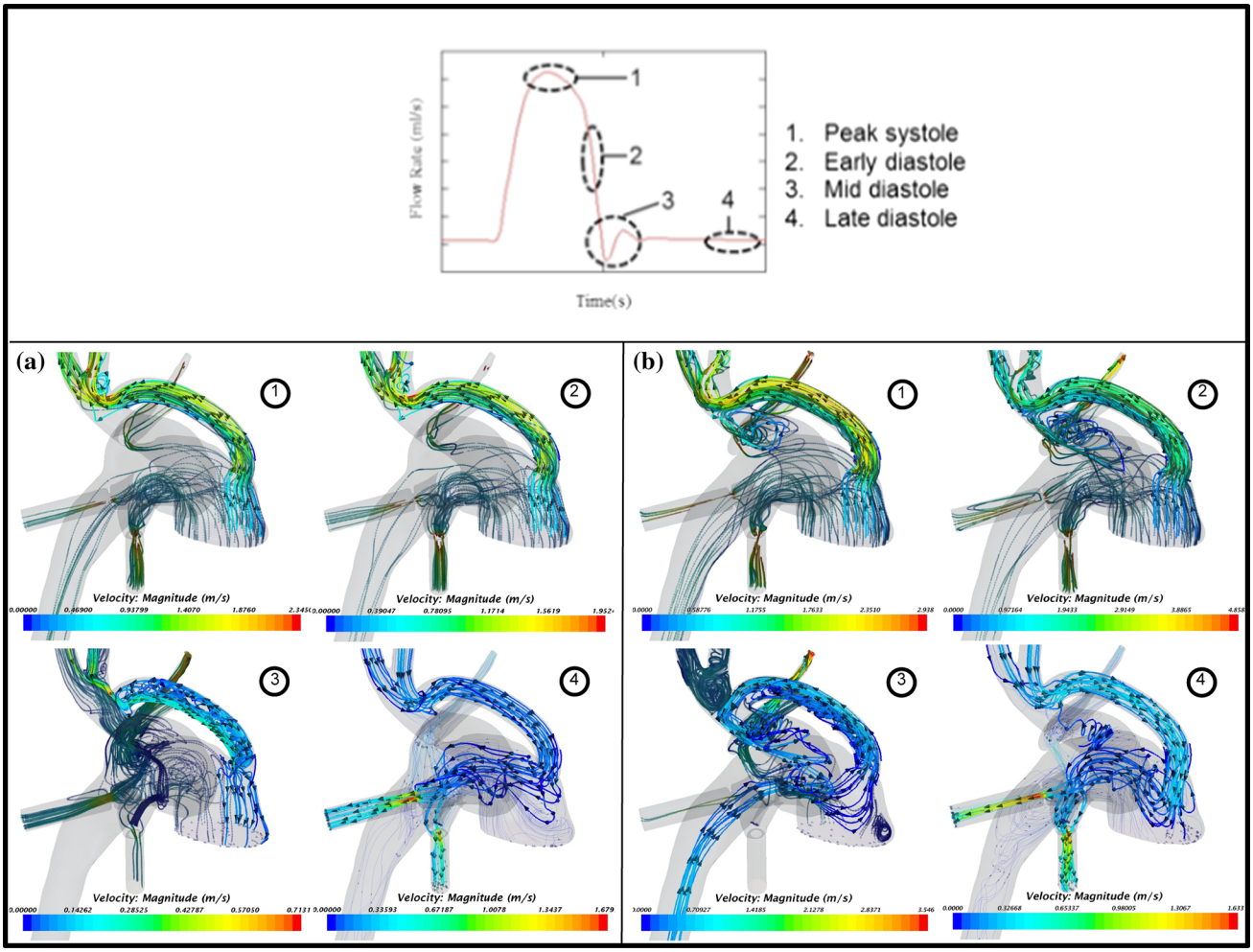

FIGURE 6. Streamlines through shunt at selected points during cardiac cycle. 4.0 mm RBTS configuration, (a) Nominal, (b) 90% stenosis.

tient-derived anatomy are less severe than the synthetic model. The Nominal 4.0 mm RBTS configuration has a more uniform flow through the shunt as compared to its synthetic analog during most of the cardiac cycle, with less formation of swirling structures. There are multiple areas of flow recirculation, most prominently in the IA root and the ascending aorta, the latter being significantly larger and more proximal to the atretic aortic valve than in the synthetic case and thus creates regions of low flow velocity and recirculation throughout the cardiac cycle. RBTS flow in late diastole in nominal configurations exhibits an interesting phenomenon in which both antegrade and retrograde flow exist within the lumen. The portion of shunt wall corresponding to the larger radius of curvature (distal to the PA) is in contact with a swirling antegrade flow, while the wall portion corresponding to the inner radius of curvature is in contact with a more uniform retrograde flow. Figure 7 provides a close-up of late diastolic shunt flow during mid-diastole (corresponding to time point 3 as indicated in Fig. 6) for patient-derived nominal cases with RBTS.

For all patient derived configurations, the flow velocity is significantly higher in the LCA due to it being severely narrowed in this anatomy as compared to the other branching arteries (an outlet RCA to LCA area ratio of 9.5). Nominal RBTS cases exhibit a less prevalent recirculation zone at the IA root and a more uniform shunt flow throughout the cardiac cycle in the Nominal 3 mm and 3.5 mm RBTS configurations. The antegrade shunt flow velocity with the 3.5 mm RBTS is lower than in the 3.0 mm RBTS configuration (Fig. 5), while the retrograde shunt flow velocity increases for decreasing shunt size.

Severely stenosed cases exhibit pronounced impingement and recirculation zones at the IA root. In general, shunt flow is more uniform as the shunt is reduced in diameter. Increased shunt flow results in increased cycle averaged and peak shunt flow velocities (Fig. 5). The increase of RBTS antegrade flow velocity

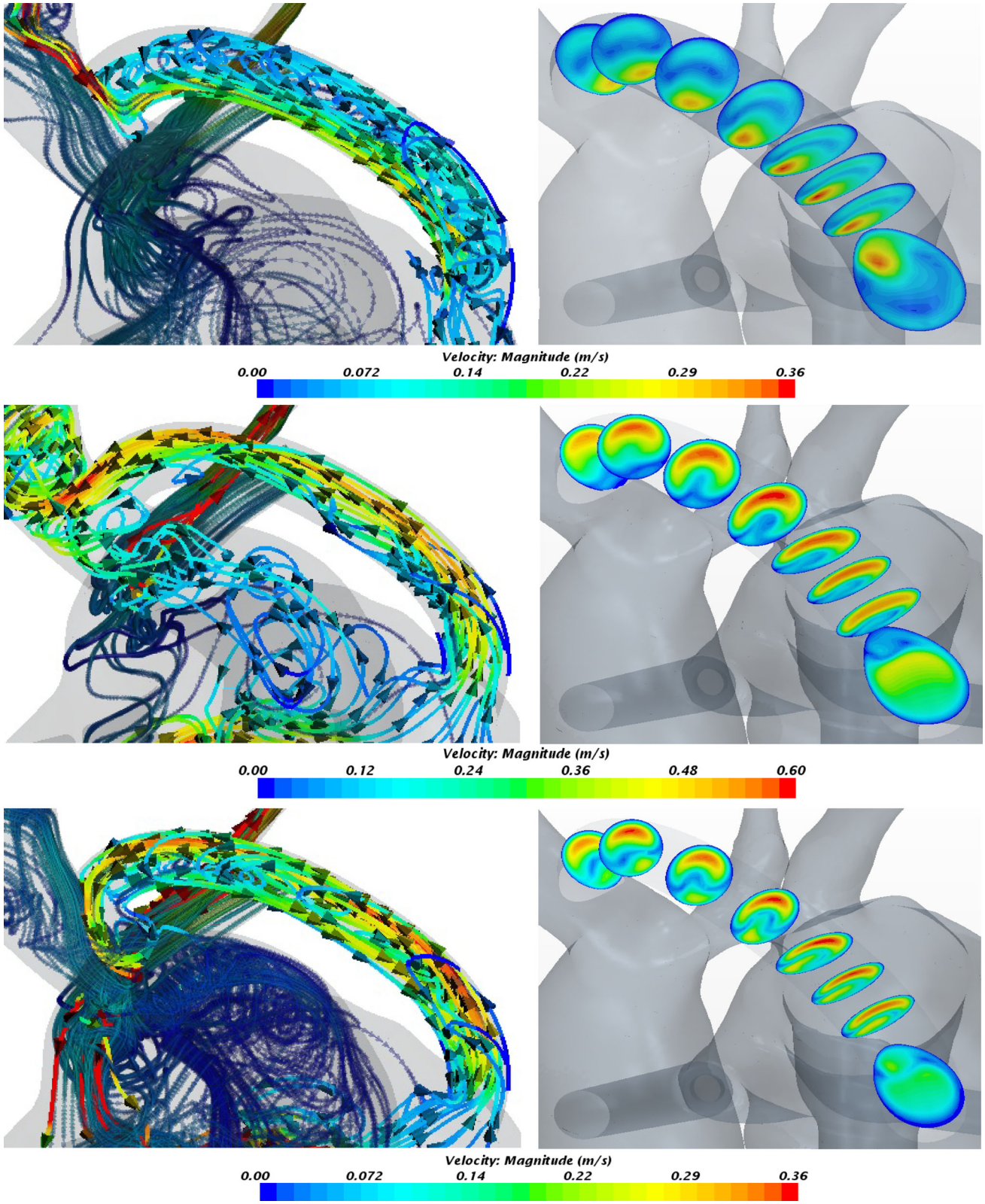

FIGURE 7. Comparison of shunt flow in mid-diastole (time point 3 as indicated in Fig. 6). Nominal patient-derived configurations with 4 mm (Top), 3.5 mm (Middle), and 3 mm (Bottom) RBTS.

over the cardiac cycle in severely stenosed cases relative to nominal cases for the same diameter is 62, 69, and 59% respectively for 3.0, 3.5, and 4.0 mm diameters. A larger increment is computed for retrograde flow velocities over the cardiac cycle, where the increase in flow through the RBTS relative to the nominal cases is 145, 166, and 148% respectively for 3.0, 3.5, and 4.0 mm diameters.

Figure 5 also offers insight in the cycle fraction of antegrade flow for each case. This can be interpreted as the portion of time the shunt experiences antegrade flow or alternatively the fraction of time in a cycle where recirculation is prominent. For large fractions of cycle antegrade flow, as for the 3 mm and 3.5 mm grafts, flow pattern presents less recirculation which can reduce the potential for thrombogenesis. In comparison, the 4 mm RBTS consistently shows lower cycle antegrade flow fractions which translate in longer presence of recirculation and larger potential for thrombogenesis. This observation may cause the 4 mm graft to be less desirable.

Another important result from the stenosed RBTS cases is that systemic flow and pressure waveform amplitudes increase relative to the Nominal RBTS and non-RBTS cases (Figs. 8, 9, 10, and 11). The opposite is true for the pulmonary arterial waveforms (Fig. 9). This results in higher forward flow during systole and higher reverse flow during diastole for the branched arteries, with a net gain in cycle arterial perfusion. Pulmonary flow on the other hand is always forward regardless of the configuration but becomes steadier in RBTS cases, with a higher flow contribution from the branched arteries during diastole (Fig. 9).

In non-RBTS cases with severe stenosis, there is considerable diastolic flow to the branched arterial beds, and most of the pulmonary flow during diastole is provided primarily by reversed flow from the DA and LSA since these vessels are proximal to the pulmonary banding sites. In severe stenosis with RBTS cases there is less restriction to systemic flow throughout the cardiac cycle and thus pulmonary flow during systole is reduced while systemic flow is increased. Furthermore, the pulmonary banding is in itself a non-linear resistance and acts to restrict flow increasingly during systole than during diastole. That is, an equivalent rise in the pressure differential across the banding during systole produces lower flow than it would during diastole. This behavior encourages systolic shunt flow to the branched arteries and thus increases the need for diastolic pulmonary flow (Fig. 10). The pulmonary diastolic flow in RBTS configurations has three instead of two sources, retrograde flow across the stenosis, the RBTS, and the DA. Since the shunt is proximal to the pulmonary banding sites, the contribution of branched arterial flow (reversed/retrograde flow) to pulmonary flow

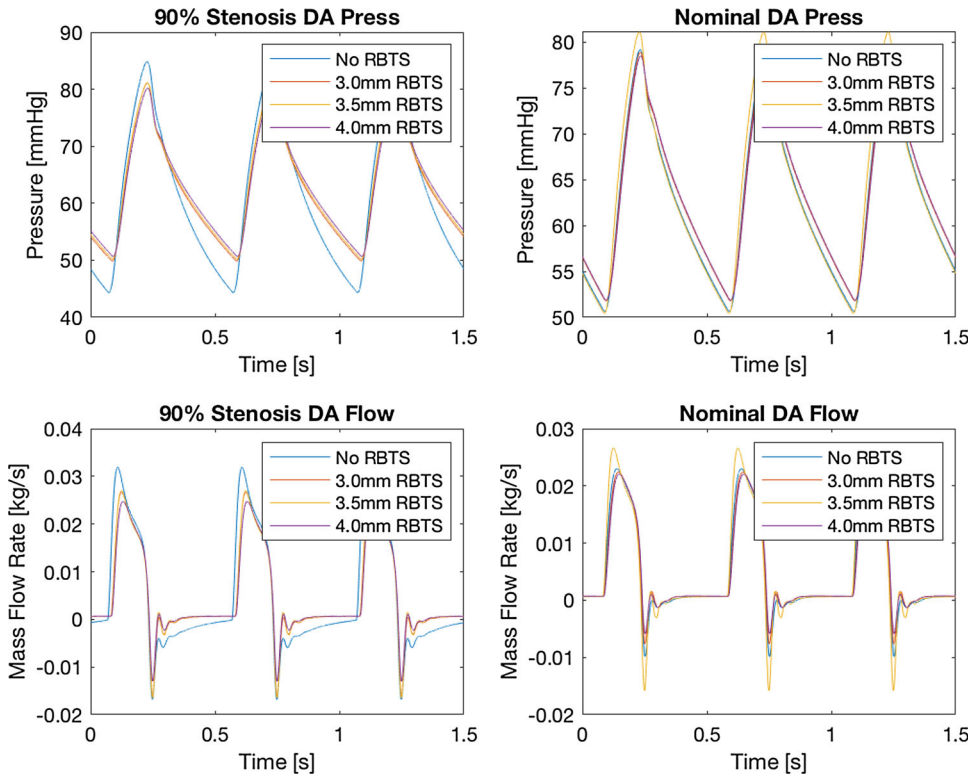

FIGURE 8. DA pressure and mass flow rate waveforms for all configurations.

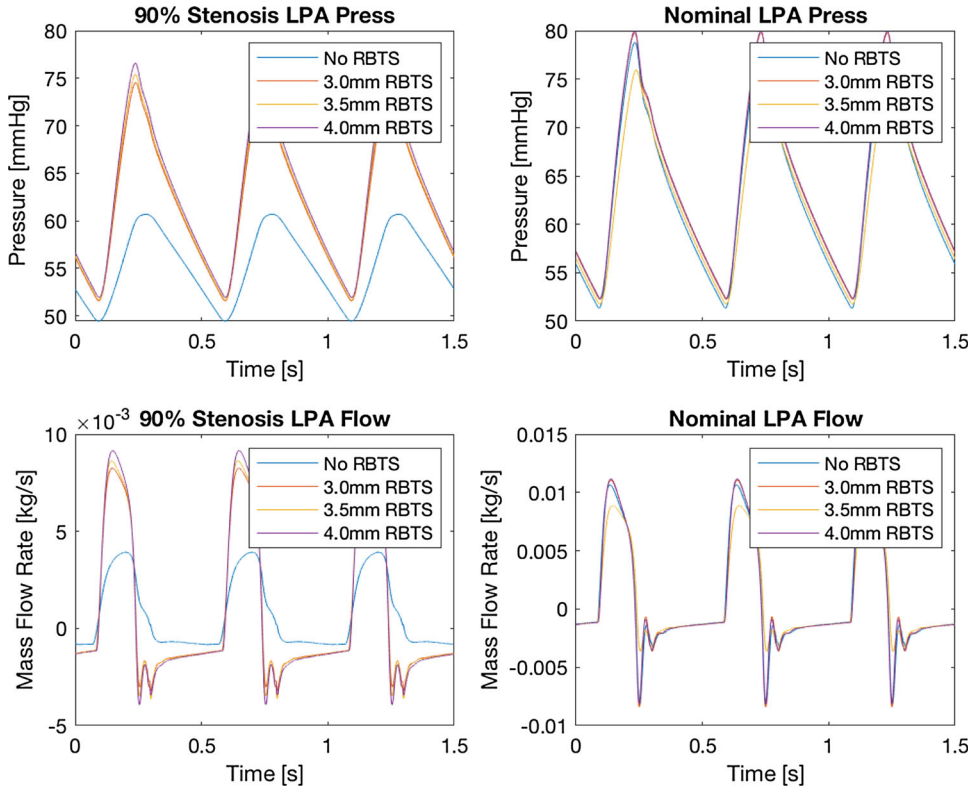

FIGURE 9. LPA pressure and mass flow rate waveforms for all configurations.

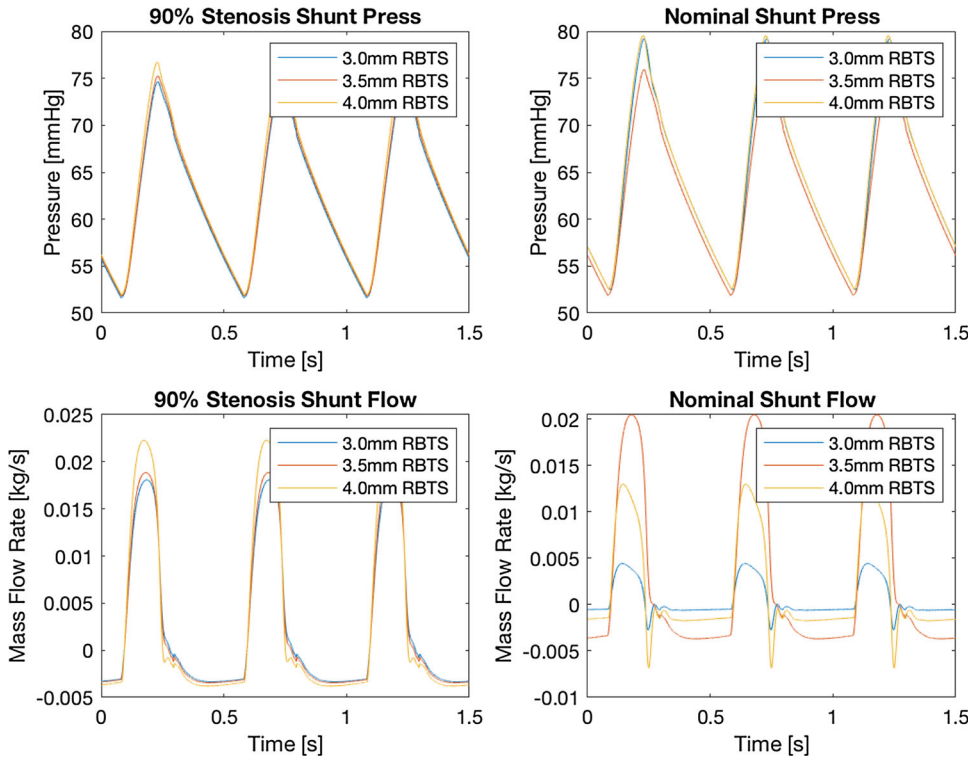

FIGURE 10. Shunt pressure and mass flow rate waveforms for all configurations.

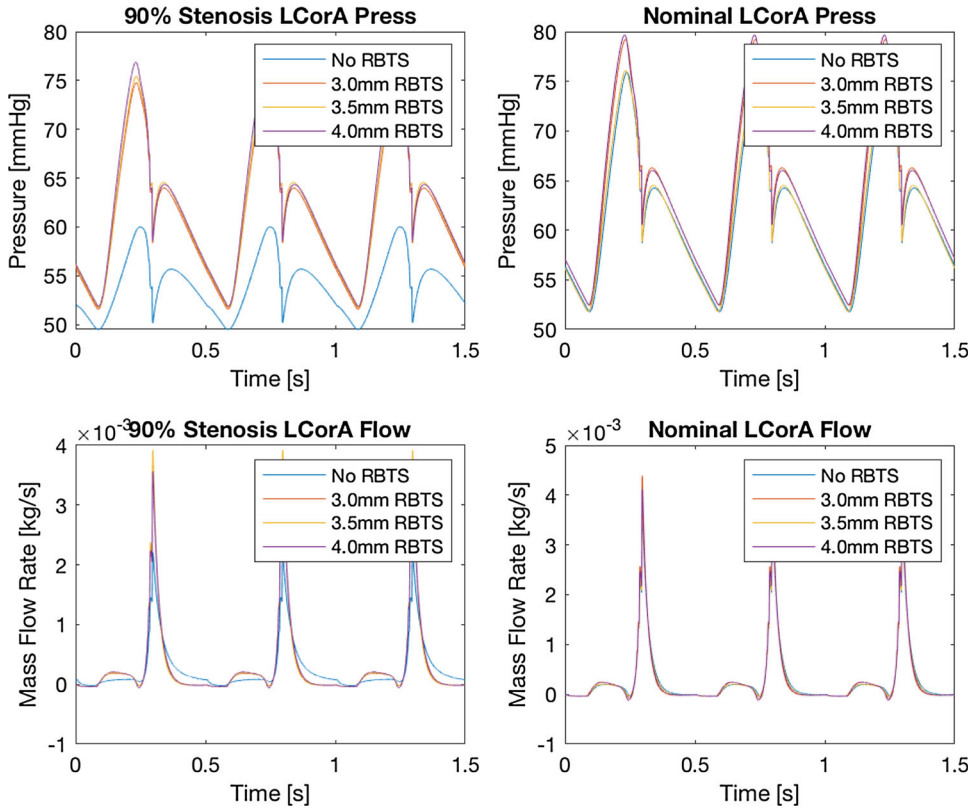

FIGURE 11. Left coronary pressure and flow waveforms for all configurations.

during diastole rises considerably and relative to DA flow.

A key result is that all three shunts restored coronary flow and pressures back to near nominal values in the presence of severe 90% stenosis. The waveforms are provided in Fig. 11 for the left coronary (the right coronary exhibits similar trends and is not displayed here). In nominal case, the presence of the RBTS shunts placed prophylactically result in slightly lower coronary pressure as compared to the no shunt case, with the 4 mm shunt resulting in the largest deviation from nominal pressure waveform.

Oxygen Transport

The maximum systemic oxygen delivery increase for the patient derived anatomies obtained by introducing the RBTS is 2.2% for nominal configurations and 8.5% for stenosed configurations (Fig. 12). In the nominal cases the implantation of a shunt does not strongly improve oxygen delivery, although the 4 mm shunt seems to the most advantageous. In the stenosed configurations the shunt greatly enhances the oxygen delivery, however the diameter used for the RBTS has little effect on overall systemic oxygen delivery, while the 4 mm shunt appears to be the best option.

Table 3 offers a closer look at the effects of the RBTS on systemic oxygen delivery. In the absence of stenosis, shunt diameter does not lead to large changes in oxygen transport. The 4 mm RBTS can be observed to induce the largest increment in oxygen transport as seen in Fig. 12. In the presence of stenosis, the introduction of the RBTS has clearly a beneficial effect for all branches. Shunt diameter seems to have a milder effect on oxygen transport with an increase in oxygen delivery observed for increasing shunt diameter. It can be observed that in the stenosed model, the graft restores oxygen delivery to nominal levels for each of the cerebral vessels. A similar effect is seen in the coronary bed as well as in the subclavians. The lower systemic circulation has only a mild enhancement of the systemic oxygen transport.

The beneficial effect on the systemic oxygen delivery can be explained by an improved perfusion of the various beds. Table 1 in conjunction with Table 3 display this effect quantitatively. The introduction of the RBTS restores flow to near nominal levels in the upper circulation, which in turn enhances oxygen delivery.

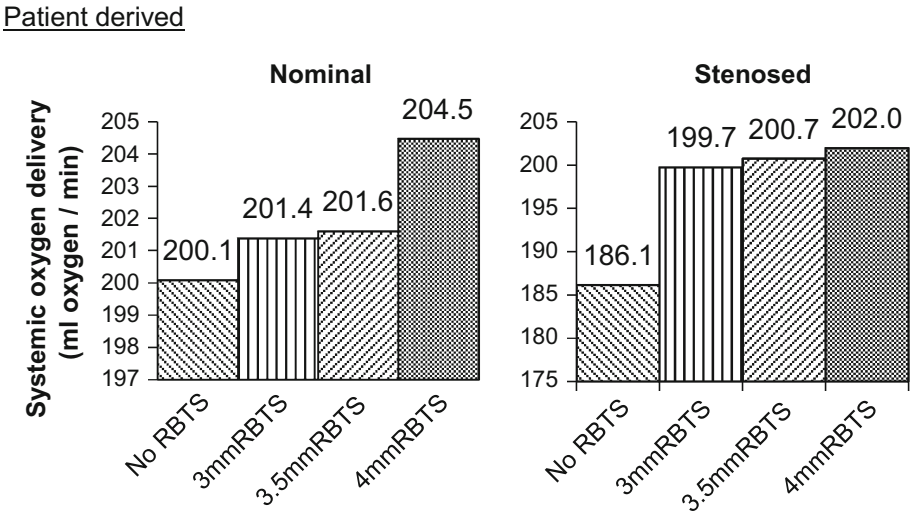

FIGURE 12. Systemic oxygen delivery for all anatomical configurations and shunt diameters.

TABLE 3. Systemic oxygen delivery based on percentile branch flow of systemic flow.

	Systemic oxygen delivery (mL oxygen/min)						
Patient derived	DA	LCA	LcorA	LSA	RCA	RcorA	RSA
Nominal	113.9	18.3	7.0	18.3	18.3	6.6	17.9
Nominal-3 mm RBTS	114.1	18.0	6.6	18.4	18.4	7.0	18.4
Nominal-3.5 mm RBTS	115.0	18.2	6.7	18.2	18.2	6.7	18.2
Nominal-4 mm RBTS	115.4	18.6	6.7	18.6	19.0	6.7	18.6
Stenosed	111.5	15.3	6.0	15.7	15.7	6.4	15.3
Stenosed-3 mm RBTS	113.9	18.0	6.7	18.0	18.0	6.7	18.0
Stenosed-3.5 mm RBTS	114.1	18.1	6.7	18.1	18.1	6.7	18.1
Stenosed-4 mm RBTS	114.8	18.2	6.7	18.2	18.2	6.7	18.2

Wall Shear Stress, Oscillatory Shear Index, and Vorticity

Of particular interest in this study is how the vessel WSS changes depending on shunt diameter. Studies[17,20,23,32] have shown a strong correlation in the magnitude of shear stress, endothelial cell function, and vessel wall remodeling. Low levels of shear stress promote platelet activation and coincide with areas of low flow velocity, typically the outer walls of bifurcations and recirculation zones. Varying levels of shear stress through the PDA, where a metallic stent is placed to prevent ductus closure, may induce the formation of neointimal hyperplasia leading to distal arch stenosis. Flow characteristics surrounding the RBTS anastomosis are also of great interest since studies have suggested that a careful selection of shunt diameter and anastomosis design can achieve greater shunt patency and reduction in graft thrombosis.[5,16] Figures 13, 14, 15 and 16 depict WSS and OSI for all RBTS configurations, with the WSS color map clipped at a top range of 30 dynes/cm^2.

All patient derived configurations exhibit very similar trends with respect to the effects of shunt diameter on WSS and OSI. The prominent areas of high WSS in all models include shunt anastomosis sites, pulmonary banding region, stenosis region, and the root of the LSA. Areas of high OSI in all models include the mid-RBTS, left and right carotid roots, stenosis region, and the DA. For both anatomical models, configurations with the 4.0 mm shunt exhibit less wall shear stress in critical regions such as the shunt anastomosis sites and stenosis surroundings (Fig. 13).

In all configurations there is a region of progressively higher WSS as the RBTS diameter decreases extending from the stenosis site retrograde through the aortic isthmus into the LCA root. The distal shunt anastomosis as well as the shunt wall also exhibit larger regions of higher WSS as the shunt diameter decreases. There is very slight OSI variability in all Nominal configurations.

In the 90% stenosis RBTS cases (Fig. 15) there is a sharp increase in WSS near the shunt anastomosis sites as well as the proximal half of the shunt in the 3.0 mm

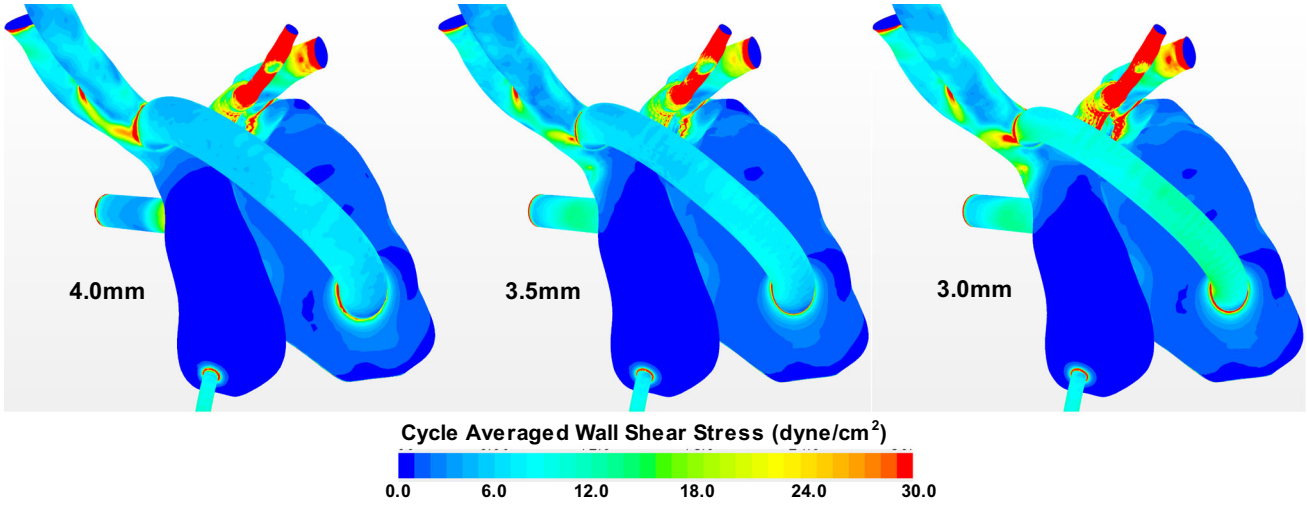

FIGURE 13. Contour plots of cycle averaged wall shear stress magnitude for the nominal (0% stenosis) case.

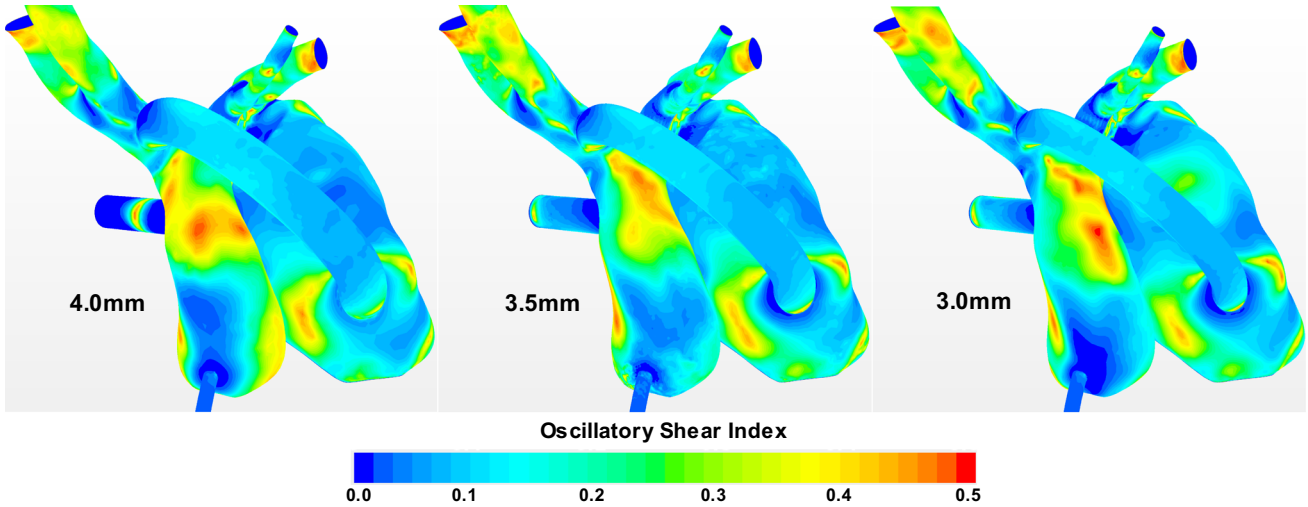

FIGURE 14. Contour plots of oscillatory shear index for the nominal (0% stenosis) case.

case relative to the 4.0 mm and 3.5 mm case. Higher WSS is also seen at the root of the LSA as shunt diameter decreases; this is due to the higher flow rate through the stenosis site impinging at the distal side of the LSA root.

It has been documented that exposure to regions of high shear stress can cause platelet activation.[28] In Fig. 15 several localized areas of high WSS (≥ 30 dyne/cm^2) can be observed proximally and distally in the graft. For the 3 mm RBTS the exposure area is larger compared to the other graft sizes which can lead to longer exposure times. Prolonged exposure to high WSS magnitudes can potentially induce thrombogenesis as well.[28] In addition, it has been shown that increased rates of platelet activation can follow changes in the WSS magnitudes that platelets may experience. Following exposure to large WSS, platelets become more 'sensitive' to lower downstream shear stresses. Figure 15 displays similar flow features for the 3 mm graft, where prolonged exposure to high WSS is followed by much lower WSS that can cause insulted platelets to become activated. Similar analyses of the 3.5 mm and 4 mm RBTS display lower potential exposure periods due to smaller high WSS areas.

Regions of peak OSI for patient derived anatomic configurations include the DA, pulmonary arteries distal to the banding, and root of the LSA and LCA (Figs. 14 and 16). There are no considerable changes in OSI due to shunt diameter for the nominal configurations. There is a notable decrease in OSI through the mid-aortic arch region and branching arteries as shunt diameter decreases in severely stenosed cases. In general, for the severely stenosed cases there is a consid-

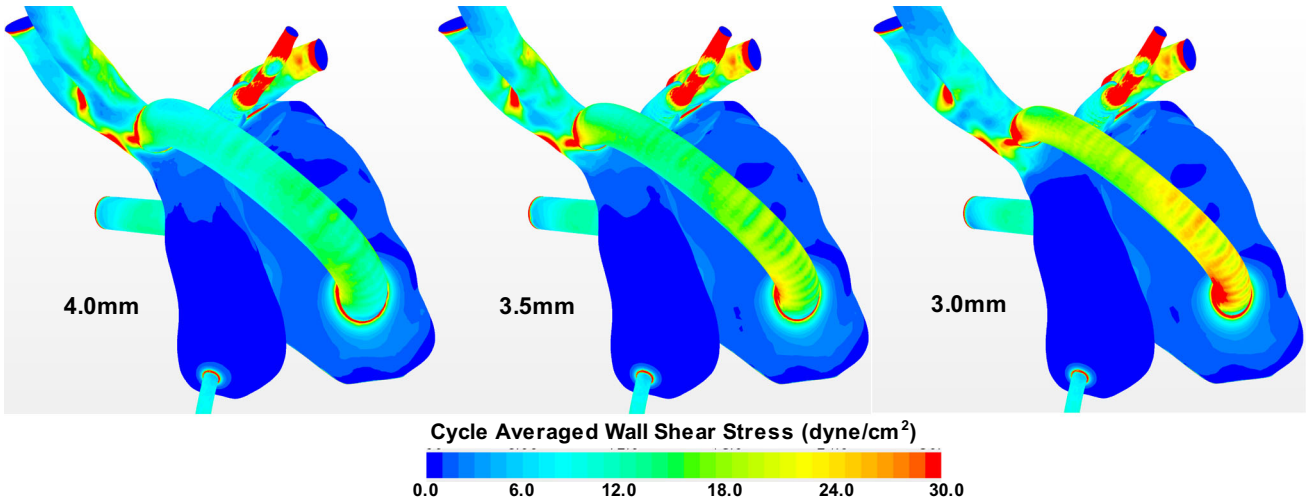

FIGURE 15. Contour plots of cycle averaged wall shear stress magnitude for the severe (90% stenosis) case.

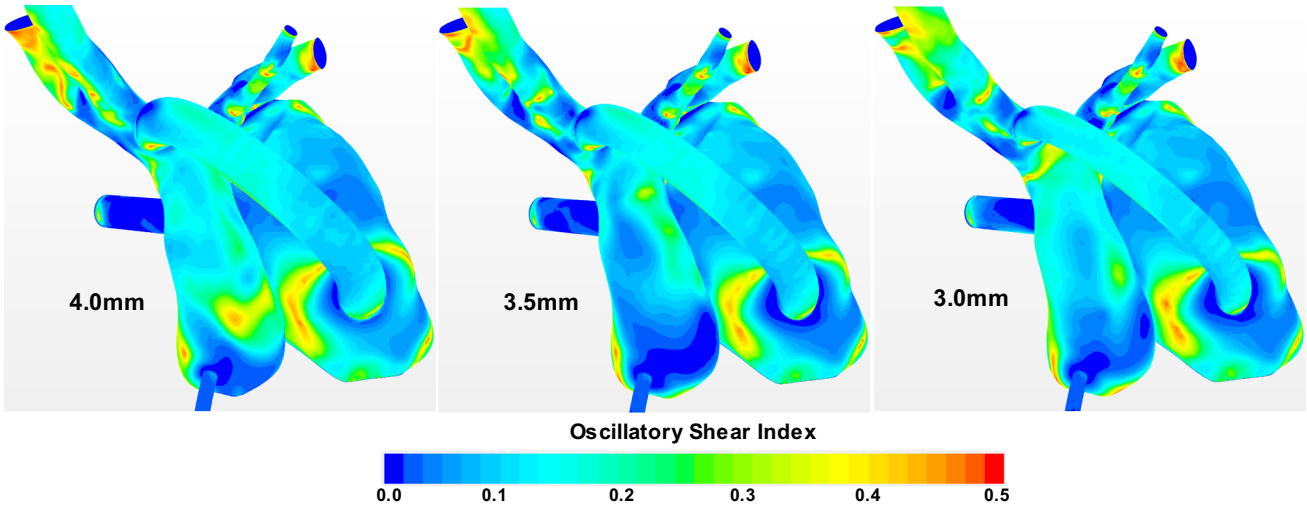

FIGURE 16. Contour plots of oscillatory shear index for the severe (90% stenosis) case.

erable reduction in OSI in the ascending aorta and DA relative to nominal configurations.

Moreover, we examined the shunt flow vorticity (a measure of fluid rotation) whose volume average value over a cardiac cycle is displayed in Fig. 17. Vorticity increases as the shunt diameter decreases; an increased velocity magnitude through the shunt increases the vorticity generated at the walls. The cycle averaged vorticity considering all shunt diameters increases from nominal to severe stenosis by 87% for patient derived cases. In this setting, where perfusion is restored to all arterial beds to near nominal levels (with similar distribution of flow in both anatomies) by the RBTS, these results suggest that shunt flow vorticity has little correlation with the patient anatomy. In other words, vorticity generation can be attributed predominantly to how much flow traverses the shunt and to shunt diameter, and not the anatomical configuration.

CONCLUSIONS

We utilized a multi-scale model to study the hemodynamics of the hybrid Norwood palliative treatment for HLHS.[9] Calculated local hemodynamics derived from the model provide insight on the effects of severe stenosis and the diameter of the implanted RBTS. This study considered the effects of varying RBTS diameters (3.0, 3.5 and 4.0 mm) and the effects of severe stenosis of the aortic isthmus by comparing nominal cases with cases having a 90% reduction in distal arch lumen. In the stenosed aortic arch, the

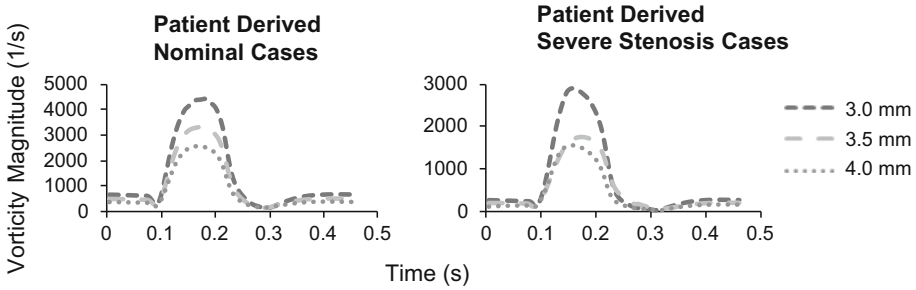

FIGURE 17. Volume averaged vorticity of flow through RBTS over one cardiac cycle.

RBTS compensated for the distal arch obstruction, restoring cardiac output as well as coronary and arch branch flows and pressures to near nominal levels. Systemic flow and pressure waveform amplitudes increase in severely stenosed cases with RBTS relative to lesser degrees of stenosis, while the opposite occurs for the pulmonary arterial waveforms. RBTS diameter has little effect on overall systemic oxygen delivery with the 4.0 mm shunt providing the greatest improvement. However, as with flow rates, the introduction of the shunt restored near nominal oxygen delivery and coronary flow and pressures when the arch is severely stenosed.

The nominal case with 4.0 mm RBTS configuration exhibits low flow velocity and disorganized flow through the shunt, which increase the possibility of thrombogenesis and hyperplasia. Cases with the 3.0 mm RBTS exhibit higher shear stress at critical sites such as shunt anastomosis and stenosis sites which may reduce shunt patency and promote vessel wall remodeling. From a clinical perspective, our results suggest that the 3.5 mm RBTS maintains acceptable hemodynamics without the deleterious patterns observed with the 3.0 and 4.0 mm shunts. The disordered flow patterns seen in late diastole with the larger shunt may lead to thrombosis. On the other hand, the smaller shunt diameters are at higher risk of suture line stenosis. However, suture-line-stenosis associated with higher levels of WSS near anastomosis sites in small diameter shunts develops gradually over time and, therefore, can be detected and corrected by balloon dilation and stenting. In case of severe stenosis, shunt flow disorder is greatly reduced. Among the three graft sizes, the best option seems to be the 3.5 mm RBTS which provides a more organized flow similar to that of the 3.0 mm configuration with lower levels of wall shear stress. As such, in the setting of this study our results suggest: (1) the 4.0 mm shunt is a generous shunt diameter choice that may be problematic particularly when implemented prophylactically in the absence of stenosis, and (2) the 3.5 mm shunt may be a more suitable alternative since it exhibits more favorable hemodynamics at lower levels of wall shear stress.

Limitations

The principal limitation of this study is the rigid-walled CFD model, which does not account for arterial compliance within its domain. However, other research groups utilizing closed-loop fluid structure interaction simulations of HLHS patients who have undergone stage one palliation concluded that a rigid-wall assumption does not significantly affect the resultant flow and stress fields.[14] The peripheral arterial compliances of the LPM model were tuned to compensate for this limitation with regards to absolute flow and pressure waveforms. Additionally, vessel wall elasticity can exaggerate impedance mismatches at vessel junctions or anastomoses, thereby affecting the flow characteristics. WSS is magnified due to the lack of compliance and thus only a relative comparison of its magnitude among the different anatomical configurations is appropriate.

FUNDING

Andres Ceballos received funding from the NIH NRSA predoctoral fellowship. Alain J. Kassab has received funding from the Orlando Health Foundation and from the American Heart Association under Grant No. 11GRNT7940011. William M. DeCampli has received funding from the American Heart Association under Grant No. 11GRNT7940011.

CONFLICT OF INTEREST

Ray Prather declares that he has no conflict of interest. Eduardo Divo declares that he has no conflict of interest.

REFERENCES

[1]Alsoufi, B., J. Bennetts, S. Verma, and C. A. Caldarone. New developments in the treatment of hypoplastic left heart syndrome. *Pediatrics* 119:109–117, 2007.

[2]Baba, K., O. Honjo, R. Chaturvedi, K. J. Lee, G. Van Arsdell, C. A. Caldarone, *et al*. ''Reverse Blalock–Taussig shunt'': application in single ventricle hybrid palliation. *J. Thorac. Cardiovasc. Surg*. 146:352–357, 2013.

[3]Baker, C. E., C. Corsini, D. Cosentino, G. Dubini, G. Pennati, F. Migliavacca, *et al*. Effects of pulmonary artery banding and retrograde aortic arch obstruction on the hybrid palliation of hypoplastic left heart syndrome. *J. Thorac. Cardiovasc. Surg*. 146:1341–1348, 2013.

[4]Barnea, O., E. H. Austin, B. Richman, and W. P. Santamore. Balancing the circulation: theoretic optimization of pulmonary/systemic flow ratio in hypoplastic left heart syndrome. *J. Am. Coll. Cardiol*. 24:1376–1381, 1994.

[5]Binns, R. L., D. N. Ku, M. T. Stewart, J. P. Ansley, and K. A. Coyle. Optimal graft diameter: effect of wall shear stress on vascular healing. *J. Vasc. Surg*. 10:326–337, 1989.

[6]Bove, E. L., F. Migliavacca, M. R. de Leval, R. Balossino, G. Pennati, T. R. Lloyd, *et al*. Use of mathematic modeling to compare and predict hemodynamic effects of the modified Blalock–Taussig and right ventricle–pulmonary artery shunts for hypoplastic left heart syndrome. *J. Thorac. Cardiovasc. Surg*. 136:312–320, 2008.

[7]Caldarone, C. A., L. Benson, H. Holtby, J. Li, A. N. Redington, and G. S. Van Arsdell. Initial experience with hybrid palliation for neonates with single-ventricle physiology. *Annals Thorac. Surg*. 84:1294–1300, 2007.

[8]Calderone, C. A., L. N. Benson, H. Holtby, and G. S. Van Arsdell. Main pulmonary artery to innominate artery shunt during hybrid palliation of hypoplastic left heart syndrome. *J. Thorac. Cardiovasc. Surg*. 130:e1–e2, 2005.

[9]Ceballos, A. A coupled CFD-lumped parameter model of the human circulation: elucidating the hemodynamics of the hybrid Norwood palliative treatment and effects of the reverse blalock-taussig shunt placement and diameter. PhD Dissertation, University of Cental Florida, 2015.

[10]Ceballos, A., I. R. Argueta-Morales, E. Divo, R. Osorio, C. A. Caldarone, A. J. Kassab, and W. M. DeCampli. Computational analysis of hybrid Norwood circulation with distal aortic arch obstruction and reverse Blalock–Taussig shunt. *Annals Thorac. Surg*. 94:1540–1550, 2012.

[11]Ceballos, A., Divo, E., I. Argueta-Morales, C. Calderone, A. Kassab, and W. Decampli. A Multi-Scale CFD Analysis of the Hybrid Norwood Palliative Treatment for Hypoplastic Left Heart Syndrome: effect of the reverse Blalock-Taussig shunt diameter. ASME Paper IMECE 2013-66856, Proceedings of the 2013 International Congress and Exposition IMECE 2013, November 15–21, San Diego, California, USA.

[12]Chandran, K. B., S. E. Rittgers, and A. P. Yoganathan. Biofluid Mechanics: The Human Circulation (2nd ed.). Boca Raton: CRC Press, 2012.

[13]Corsini, C., G. Biglino, S. Schievano, T.-Y. Hsia, F. Migliavacca, G. Pennati, *et al*. The effect of modified Blalock–Taussig shunt size and coarctation severity on coronary perfusion after the Norwood operation. *Ann. Thorac. Surg*. 98:648–654, 2014.

[14]Esmaily, M., B. Murtuza, T. Hsia, and A. Marsden. Simulations reveal adverse hemodynamics in patients with multiple systemic to pulmonary shunts. *ASME J. Biomech. Eng*. 137(3):031001-1–031001-12, 2015.

[15]Galantowicz, M., J. P. Cheatham, A. Phillips, C. L. Cua, T. M. Hoffman, S. L. Hill, *et al*. Hybrid approach for hypoplastic left heart syndrome: intermediate results after the learning curve. *Ann. Thorac. Surg*. 85:2063–2071, 2008.

[16]Ghista, D. N., and F. Kabinejadian. Coronary artery bypass grafting hemodynamics and anastomosis design: a biomedical engineering review. *Biomed. Eng. Online* 12:129, 2013.

[17]Goubergrits, L., K. Affeld, E. Wellnhofer, T. Holmer, *et al*. Estimation of wall shear stress in bypass grafts with computational fluid dynamics method. *Int. J. Artif. Organs* 24:145–151, 2001.

[18]Gutgesell, H. P., and J. Gibson. Management of hypoplastic left heart syndrome in the 1990s. *Am. J. Cardiol*. 89:842–846, 2002.

[19]Hsia, T.-Y., D. Cosentino, C. Corsini, G. Pennati, G. Dubini, and F. Migliavacca. Use of mathematical modeling to compare and predict hemodynamic effects between hybrid and surgical Norwood palliations for hypoplastic left heart syndrome. *Circulation* 124:S204–S210, 2011.

[20]Kroll, M. H., J. D. Hellums, L. V. McIntire, A. I. Schafer, and J. L. Moake. Platelets and shear stress. *Blood* 88:1525, 1996.

[21]Laganà, K., R. Balossino, F. Migliavacca, G. Pennati, E. L. Bove, M. R. de Leval, *et al*. Multiscale modeling of the cardiovascular system: application to the study of pulmonary and coronary perfusions in the univentricular circulation. *J. Biomech*. 38:1129–1141, 2005.

[22]Liu, J., Q. Sun, H. Hong, Y. Sun, J. Liu, Y. Qian, *et al*. Medical image-based hemodynamic analysis for modified Blalock–Taussig shunt. *J. Mech. Med. Biol*. 15(3):1550035, 2015.

[23]Loth, F., S. A. Jones, C. K. Zarins, D. P. Giddens, R. F. Nassar, S. Glagov, *et al*. Relative contribution of wall shear stress and injury in experimental intimal thickening at PTFE end-to-side arterial anastomoses. *J. Biomech. Eng*. 124:44–51, 2002.

[24]Malek, A. M., S. L. Alper, and S. Izumo. Hemodynamic shear stress and its role in atherosclerosis. *J. Am. Med. Assoc*. 282:2035–2042, 1999.

[25]Migliavacca, F., K. Laganà, G. Pennati, M. R. de Leval, E. L. Bove, and G. Dubini. Global mathematical modelling of the Norwood circulation: a multiscale approach for the study of the pulmonary and coronary arterial perfusions. *Cardiol. Young* 14:71–76, 2004.

[26]Migliavacca, F., G. Pennati, G. Dubini, R. Fumero, R. Pietrabissa, G. Urcelay, *et al*. Modeling of the Norwood circulation: effects of shunt size, vascular resistances, and heart rate. *Am. J. Physiol*. 280:H2076–H2086, 2001.

[27]Moghadam, M. E., F. Migliavacca, I. E. Vignon-Clementel, T. Y. Hsia, A. L. Marsden, and M. C. H. Allianc. Optimization of shunt placement for the norwood surgery using multi-domain modeling. *J. Biomech. Eng. Trans. ASME* 134(5):051002, 2012.

[28]Sheriff, J., D. Bluestein, G. Girdhar, and J. Jesty. High-shear stress sensitizes platelets to subsequent low-shear conditions. *Ann. Biomed. Eng*. 38(4):1442–1450, 2010.

[29]Simaan, M. A., A. Ferreira, S. Chen, J. F. Antaki, and D. G. Galati. A dynamical state space representation and performance analysis of a feedback-controlled rotary left ventricular assist device. *IEEE Trans. Controls Syst. Technol*. 17:15–28, 2009.

[30]Stoica, S. C., A. B. Philips, M. Egan, R. Rodeman, J. Chisolm, S. Hill, *et al*. The retrograde aortic arch in the

hybrid approach to hypoplastic left heart syndrome. *Ann. Thorac. Surg*. 88:1939–1947, 2009.
[31]Waite, L. Applied Biofluid Mechanics. New York: McGraw Hill Professional, 2007.
[32]Waniewski, J., W. Kurowska, J. K. Mizerski, A. Trykozko, K. Nowiński, G. Brzezińska-Rajszys, *et al*. The effects of graft geometry on the patency of a systemic-to-pulmonary shunt: a computational fluid dynamics study. *Artif. Organs* 29:642–650, 2005.